

# Free-standing porous silicon single and multiple optical cavities

M. Ghulinyan,<sup>a)</sup> C. J. Oton, G. Bonetti, Z. Gaburro, and L. Pavesi

*INFN and Dipartimento di Fisica, University of Trento, Via Sommarive 14, I-38050 Povo (Trento), Italy*

(Received 3 March 2003; accepted 9 April 2003)

Porous silicon free-standing microcavity structures, with different layer designs, have been fabricated. Single microcavities show transmission resonances in the technologically relevant wavelength region of  $1.55\ \mu\text{m}$  with quality factors up to 3380. High-order cavities show sub-nm transmission peaks over the whole stop band. Coupled microcavity structures, where splitting of the degenerate cavity mode occurs, lead to multiple transmission peaks in a limited region of the stop band. We also report incident angle-dependent measurements, where transmission peak blueshift and splitting of transverse electric and transverse magnetic polarized modes due to porous silicon birefringence were observed. © 2003 American Institute of Physics. [DOI: 10.1063/1.1578170]

## I. INTRODUCTION

During the last decade, the optical properties of porous silicon (PS) have become a very intense area of research.<sup>1</sup> The fabrication of one-dimensional photonic structures based on PS by means of modulation of the electrochemical etching current has driven applications of this material, such as dielectric mirrors,<sup>2</sup> microcavities,<sup>3</sup> and waveguides.<sup>4</sup> All-silicon Fabry–Perot optical microcavities (MCs), with a  $\lambda/2$  layer (optical thickness) sandwiched between distributed Bragg reflectors (DBRs), consisting of alternating layers of high and low refractive indices, were made and characterized.<sup>5,6</sup> The directionality, narrowing, and enhancement of both the photoluminescence<sup>7</sup> and electroluminescence<sup>8</sup> have been reported for PS MC light-emitting devices. Infiltration with liquid crystals was performed and properties of electrically tunable PS active mirrors were discussed.<sup>9</sup> Recently, Reece *et al.*<sup>10</sup> reported the observation of subnanometer linewidths in MCs based on PS. The electrochemical etching of highly doped *p*-type Si was carried out at low temperatures ( $-22.5\ ^\circ\text{C}$ ) and resonances with subnanometer linewidths around the wavelength of 900 nm were realized.

MCs can act as highly selective wavelength filters. The typical figure of merit of a Fabry–Perot filter is its quality factor  $Q = \lambda/\Delta\lambda$ , where  $\lambda$  is the wavelength of the resonance peak, and  $\Delta\lambda$  is the resonance peak width. As an example, filters with high-quality wavelength selection are required for dynamic gain equalization in optical networks. Such application requires devices working in the standard window of minimal optical fiber attenuation, i.e., in the  $1.55\ \mu\text{m}$  wavelength region.<sup>11</sup> It is also interesting to remark that gain equalization for optical networks with wavelength division multiplexing requires a tunable wavelength as additional feature.<sup>11</sup> A simple way to tune Fabry–Perot resonance is changing the angle of incidence.

In this article, we show that subnanometer linewidths can be obtained in free-standing PS MCs, tuned to the optical

network wavelength ( $1.55\ \mu\text{m}$ ). In order to emphasize the flexibility of PS MCs fabrication process, we demonstrate the realization of various structures. The structures presented here are two single MCs (Fabry–Perot filters with an optical thickness of the spacer equal to, respectively,  $\lambda$  and 27 times  $\lambda$ ), and a structure composed of 10 coupled MCs (CMCs). The interest of CMCs is in the splitting of the cavities degeneracy, as already shown in two CMC structures.<sup>12</sup> Recently, we have shown free-standing PS up to ten CMC structures, consisting of more than 100 layers.<sup>13</sup> As will be shown next, both high-order MC structures (such as the single  $27\lambda$  MC) and the CMCs have multiple transmission resonances, although originated by totally different physical mechanisms. In addition, the optical properties of PS layers (i.e., refractive index or absorption) can change in the presence of certain gases and vapors. When these changes occur in the active layer of a MC with a high  $Q$  factor, they become much more significant, allowing high-performance gas sensors.<sup>14</sup> In this work, we demonstrate that electrochemical etching of silicon, besides its low cost, allows the fabrication of good-quality optical devices.

## II. EXPERIMENT

We have used *p*<sup>+</sup>-type ( $0.01\ \Omega\text{cm}$ ) doped Si(100)-oriented substrates. Anodization was performed at a room temperature in a solution of 30% volumetric fraction of aqueous HF (48 wt %) with ethanol. The current density was controlled by a computer controlled Keithley 2400 current/voltage source. High porosity  $\lambda/4$  layers, called *H* layers, were obtained with a current density of  $50\ \text{mA}/\text{cm}^2$  for a time of 5.9 s; they had an effective refractive index  $n_H \sim 1.4$ . Low porosity  $\lambda/4$  layers, called *L* layers were obtained with  $7\ \text{mA}/\text{cm}^2$  for 21.5 s, which results in an effective refractive index  $n_L \sim 2.1$ . Layers *H* and *L* were periodically repeated to form DBRs. We created both  $\lambda/2$  and  $\lambda$  optical cavities using the same current density as for *H* layers but with twice and four times longer duration, respectively. The structures were designed to show microcavity resonances at  $\lambda \sim 1.55\ \mu\text{m}$ . The  $\lambda$ -cavities provide thinner resonances than the  $\lambda/2$  ones. An etch-stop step of zero current was applied

<sup>a)</sup> Author to whom correspondence should be addressed; electronic mail: mghool@science.unitn.it

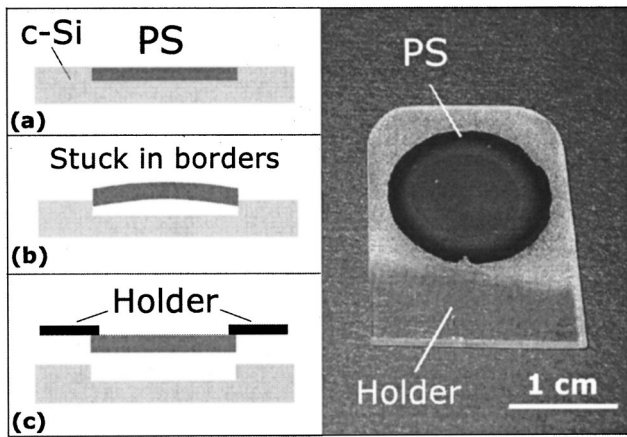


FIG. 1. Schematic diagram of free-standing PS microcavity sample fabrication (left-hand side panel): (a) before the high current step, (b) after the high current step, and (c) taking PS off the substrate after drying. A photograph of a free-standing PS coupled microcavity (right-hand side panel).

for 1 s after each layer formation to allow HF concentration regeneration.<sup>15</sup> In addition, a magnetic stirrer was used in order to enhance the exchange of solution during the whole duration of the etching process. This allowed us to grow structures with more than 110 layers without observable natural drifts in the growth direction, thus skipping the consideration of high values of artificial drifts, which were used before to compensate for the thick multilayer structures.<sup>13</sup>

An anodic electropolishing current pulse (0.4 A/cm<sup>2</sup> for 2 s) was applied at the end of the growth to detach the structure from the substrate. The sample remained stuck to the substrate in the borders, thus allowing an easy drying procedure. After rinsing in ethanol and pentane, successively, and drying in air, the structures were pasted on a plastic holder, thus obtaining free-standing PS structures. The schematic diagram of the aforementioned procedure and an optical photograph of a free-standing CMC are presented in Fig. 1. The high optical quality of the microcavities is confirmed by the transmission measurements, which we will detail in the following. The availability of free-standing structures allows us to measure the transmission of the samples in contrast with the more commonly used reflectivity measurements.

Cross-sectional scanning electron microscopy (SEM) analysis of the multilayer structures demonstrates flat interfaces between the layers (Fig. 2). As SEM does not provide information on the concomitant variation of the refractive index, the optical parameters of CMCs were investigated by transmission (*T*) measurements.

The optical characterization of PS microcavities was carried out in two different setups. A Varian Cary-5000 ultraviolet-visible-near-infrared (UV-VIS-NIR) spectrophotometer with halogen VIS-NIR lamp source and a collimated beam spot size of 1 mm was used to obtain transmission and reflection spectra in a wide range of wavelengths (800–2500 nm). The overall wavelength resolution of the system was 2 nm.

A second setup was developed for more detailed transmission measurements with a NetTest TUNICS-BT 1560 IR tunable laser in the wavelength range from 1500 to 1610 nm.

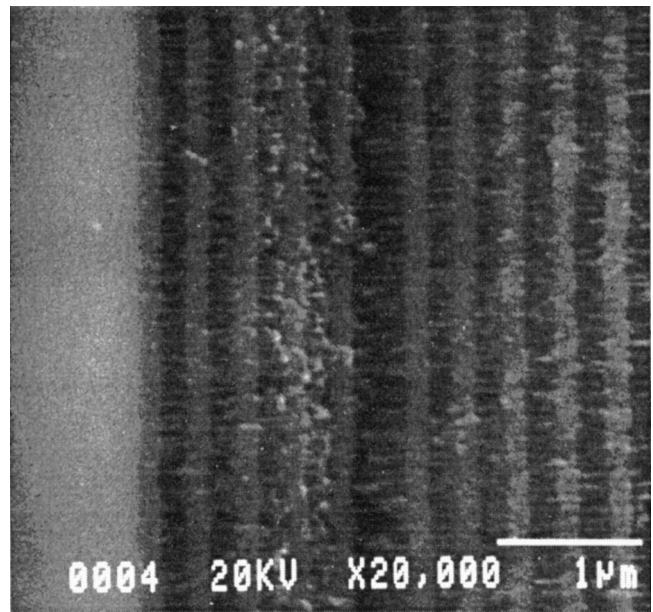


FIG. 2. Cross-sectional SEM micrograph of a few periods of a PS multilayer structure. Flat interfaces between the high (dark gray) and low (light gray) porosity layers are observable. The silicon substrate can be seen on the left-hand side.

The laser was coupled to a multimode fiber of 115  $\mu\text{m}$  diameter (Fig. 3). We used a microscope 25 $\times$  objective to focalize the laser beam in a spot of 35  $\mu\text{m}$  diameter on the sample surface. This way we were able to illuminate a very small area on the sample, thus highly reducing the broadening of peaks due to lateral inhomogeneities. A 1 mm diameter pinhole was placed just after the objective in order to reduce the numerical aperture of the input light. A fiber bunch was placed far from the sample ( $\sim 15\text{--}20$  cm) which allowed us to collect the signal with a very small numerical aperture ( $\sim 0.0075$ ). An InGaAs detector coupled to the fiber bunch was used to measure the transmitted intensity. The sample was mounted on a rotating table to carry out angle-dependent transmission measurements. The tunable laser, ro-

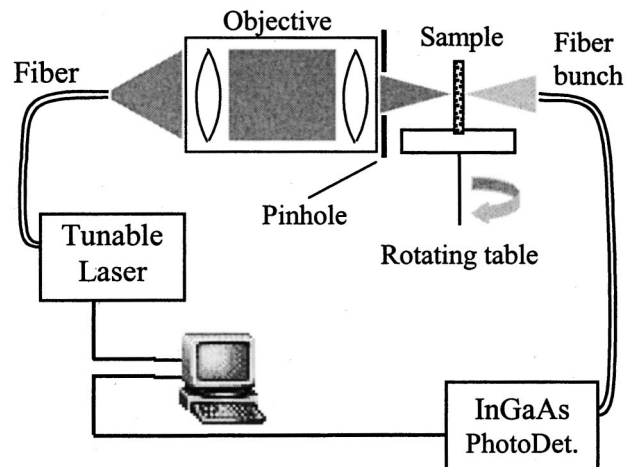


FIG. 3. Schematic diagram of the small-spot transmission setup with tunable laser operating in the wavelength range between 1.5 to 1.6  $\mu\text{m}$  (the different optical components have been drawn not in scale).

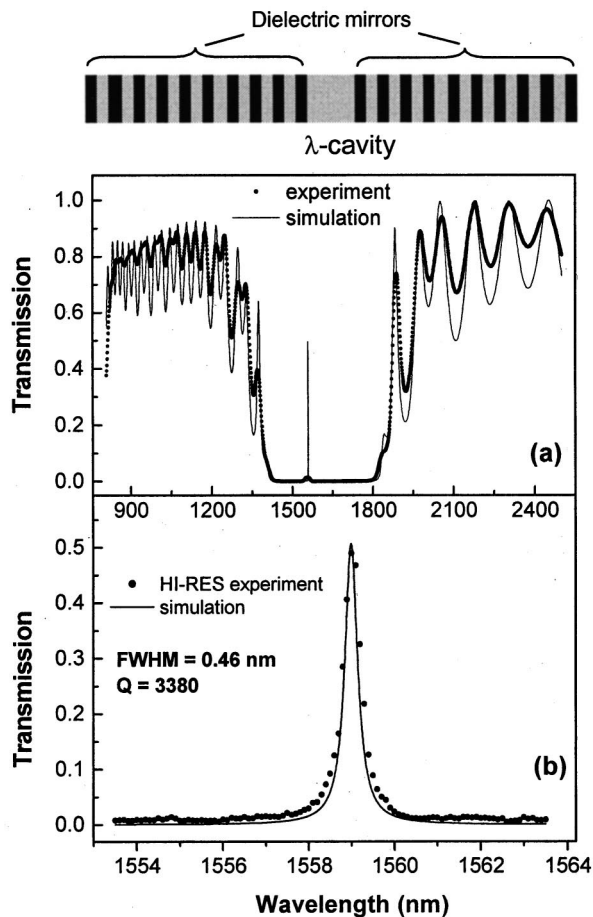


FIG. 4. Transmission spectra of a single  $\lambda$  microcavity: Solid dots are the experimental data and the lines are the simulations: (a) Measurements with 1 mm spot in a wide wavelength range, (b) measurements with  $35\ \mu\text{m}$  spot with a high-resolution tunable laser source. The top diagram shows the structure of the microcavity.

tating table, and the InGaAs photodetector were interface controlled through a computer. The transmission spectra were normalized with respect to the signal recorded without the sample.

### III. SINGLE MICROCAVITY

In Fig. 4, the schematic structure (top) and the normal incidence transmission spectra of a single  $\lambda$ -cavity, sandwiched between 9.5 period DBRs, are presented. Figure 4(a) shows the transmission spectrum measured in a wide spectral range with the spectrophotometer. Here, one can notice the wide stop band between 1300–1800 nm and the sharp resonance at about 1560 nm. More precise measurements of the transmission resonance can be carried out with the setup sketched in Fig. 3. Figure 4(b) shows the transmission spectrum recorded by this setup, where a narrow resonance peak at 1559 nm with a transmission of 50% is observed. The Lorentzian fit of these data gives a linewidth [full width at half maximum (FWHM)] of 0.46 nm which corresponds to a  $Q$  factor higher than 3380. This sharp resonance compared with the broad peak of Fig. 4(a) demonstrates the importance of illuminating a small area on the sample as well as reducing the numerical aperture of the collecting system.

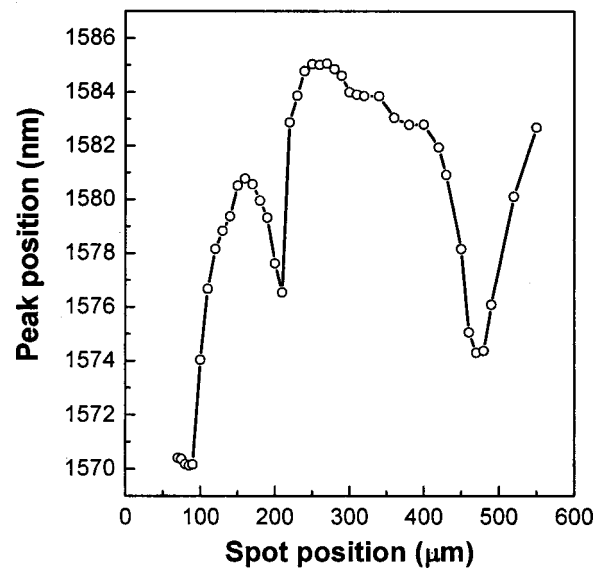


FIG. 5. Microcavity peak position dependence on the spot position on the sample surface. An illuminating spot size of  $35\ \mu\text{m}$  was used.

Using the transfer-matrix method,<sup>16</sup> the propagation of light through a PS multilayer structure can be simulated.<sup>17</sup> Numerical calculations of the transmission spectra (Fig. 4, lines) have been carried out to reproduce the experimental data. Good results for both upper and lower graphs in Fig. 4 are obtained with the nominal growth parameters for the thickness and with refractive index values of 1.43 and 2.15 for the  $H$  and  $L$  layers, respectively.

The simulation of the transmission spectrum of an ideal (no losses) structure predicts a FWHM of 0.12 nm. The best fit was obtained considering an optical loss coefficient of  $146\ \text{cm}^{-1}$  at the peak wavelength. As the microcavity is centered in the infrared where PS is almost transparent, the absorption losses play a much less important role than other loss mechanisms, such as light diffusion or scattering by the pores and by the interfaces between layers. Note that no disorder or inhomogeneities have been introduced to fit the resonance linewidth and intensity as was commonly done in the past.<sup>12</sup> This is due to probing a very small spot on the sample.

Doping inhomogeneities, which occur during the growth of the Si wafers, cause laterally inhomogeneous electrochemical etching.<sup>10</sup> As a result, the porosity of the layers varies in the plane of the sample surface. These inhomogeneities can be observed as concentric colored lines on the sample surfaces. Figure 5 reports the effect of these doping variations on the microcavity resonance position. The peak position shifts of more than 15 nm within a  $200\ \mu\text{m}$  region. This fact demonstrates the importance of the use of a very small spot size to accurately measure the optical spectra of PS microcavities.

We have observed that the microcavity mode peak slightly blueshifts with time due to the aging of the sample. Oxidation of the pore walls in air occurs and the effective refractive indices of the porous layers slightly decrease. This reduces the optical path and, consequently, blueshifts the cavity peak. Figure 6 shows the peak position change of a microcavity structure as a function of time. An exponential

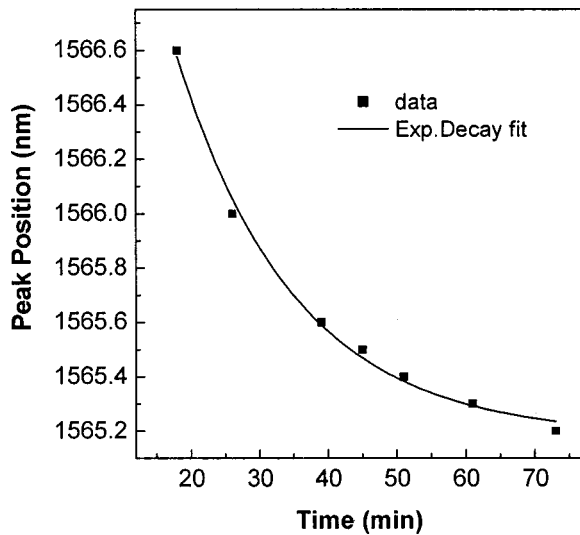


FIG. 6. Microcavity peak shift in time due to oxidation in air ( $t=0$  corresponds to the start of the drying procedure).

fit of the data is also shown in Fig. 6. The resonance peak of cavity shifts about 1.5 nm, which means that the change in the effective refractive index of the cavity layer is very small. This is consistent with the fact that in PS formed on highly doped *p*-type Si substrates, the extent of oxidation is of the order of  $\sim 1\%$ .<sup>18</sup> The microcavity peak shift saturates in time, and after 1 h, stable conditions are reached.

PS is known to be an optically anisotropic material.<sup>19,20</sup> The observation of strongly anisotropic scattering of laser light at oblique incidence on a (100)-oriented PS layer was reported recently and positive birefringence was observed.<sup>21</sup> We have carried out also incident angle-dependent transmission measurements of our structures. As expected, the microcavity peak blueshifted when the incident angle was increased. Moreover, a splitting of cavity mode at high incident angles was observed (Fig. 7). As the refractive indices for the ordinary and extraordinary modes differ, splitting of transverse-electric (TE) and transverse-magnetic (TM) polarized modes occurs, and different shifts of the resonance are observed in the transmission spectra.  $(\lambda_0^{\text{ord}} - \lambda_0^{\text{ext}}) \sim 6$  nm at  $15^\circ$  angle. We believe that the widening and decrease in the intensity of the peaks for bigger angles are mainly due to the stronger light scattering when the pores are illuminated obliquely, as well as the increase of probing spot area.

#### IV. COUPLED MICROCAVITIES

We also fabricated multiple cavity PS free-standing multilayers. These are formed by a series of equal cavity layers separated by internal DBRs (or coupling DBRs) and embedded within two external DBRs (see the top schematic structure in Fig. 8).<sup>12</sup> Optical coupling between the various cavities yields a splitting in the cavity modes with the appearance of multiple resonances within the stop band.

Structures with two, seven, and ten CMCs were produced. These structures had the following sequence of alternating high and low porosity layers:  $LHLHLHLHL$   $(HH)_1LHLHLHLHL$   $(HH)_2 \dots (HH)_n LHLHLHLHL$ ,

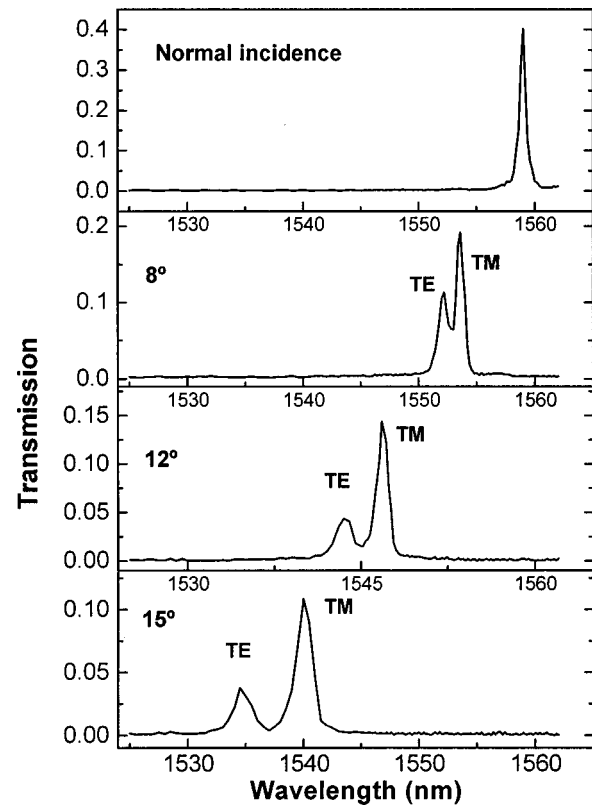


FIG. 7. Incident angle dependence of the single microcavity resonance mode. The splitting of the TE and TM polarized modes is observed.

where  $(HH)_n$  denotes the  $n$ th  $\lambda/2$  cavity. We designed the internal DBRs to have 4.5 periods in order to obtain weak coupling.<sup>13</sup>

As mentioned herein, a magnetic stirrer was used during the sample preparation. We have considered 10% and 4% thickness changes for deeper *H* and *L* layers, respectively, to compensate for the natural drifts. This is easily achieved by varying the duration of etch.<sup>13</sup> In Fig. 8(a), the transmission spectrum of a ten CMC structure (dots) measured with the spectrophotometer is presented. The structure shows a  $\sim 800$  nm wide stop band and the coupled cavity modes within. Figure 8(b) shows the transmission spectrum (dots) of the same structure taken with the tunable laser setup. Narrow transmission peaks due to the coupled optical modes with a splitting of 14 nm ( $\pm 1$  nm) are observed. Only eight transmission resonances are observed due to the limited wavelength region of the setup. Maximum transmission of 55% was obtained.

The simulation of data in Fig. 8(a) yields refractive index values of 1.43 and 2.13 for the first high and low porosity layers. Though the same currents and etching times were used for CMCs and the single microcavities of Fig. 4, slight differences in the refractive index are expected due to the inhomogeneous doping of the wafers. A 10% total negative linear drift in the refractive index of the layers through the structure growth direction was also considered. This is due to the fact that the porosity in the layers changes with depth. This effect has been observed experimentally<sup>22,23</sup> and investigated theoretically<sup>24</sup> in the past. The higher porosity values

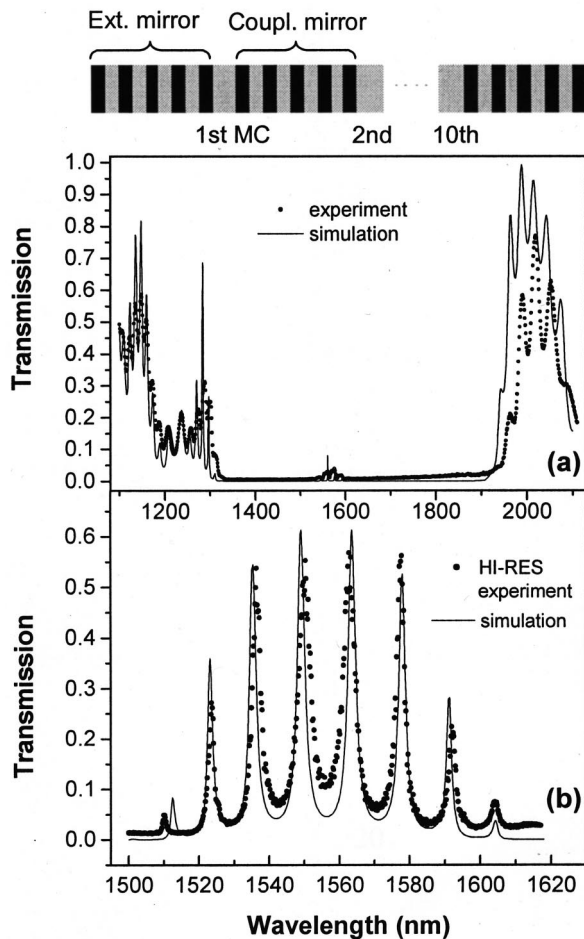


FIG. 8. Transmission spectra of a ten coupled microcavity structure, with  $\lambda/2$  cavities sandwiched between 4.5 period external DBRs (dots) and numerical calculations (lines): (a) Wide range measurements with 1 mm spot size and (b) high-resolution measurement with  $35 \mu\text{m}$  diameter spot. The top diagram shows the structure of the coupled microcavities.

of the top layers can be explained by considering the lateral increase of the pore dimensions caused by the long stay time in the electrolyte of the layers formed at the beginning of the electrochemical attack. An overall agreement of the simulations with the experimental data can be observed in Fig. 8(a).

A slightly different set of parameters has been used to reproduce the data of Fig. 8(b) as the measurements were performed in different setups, therefore locally, the structure can be different due to the doping inhomogeneity of the wafer. Numerical simulations of spectrum shown in Fig. 8(b) yield to similar refractive index values for the top layers as those used to fit Fig. 8(a) except for only a 4% negative drift of  $n_H$  of  $H$  layers. The good agreement with experimental data found justifies the accuracy of the considered fitting parameters (Fig. 8, lines).

## V. LARGE SPACER MICROCAVITY

We have fabricated also a PS-based Fabry–Perot interference filter, where a high porosity cavity layer of  $27\lambda$  optical thickness ( $\lambda=1.55 \mu\text{m}$ ) was sandwiched between two 5.5 period DBRs, as shown in the top schematic structure in Fig. 9. The whole structure was  $35 \mu\text{m}$  thick. Due to the high

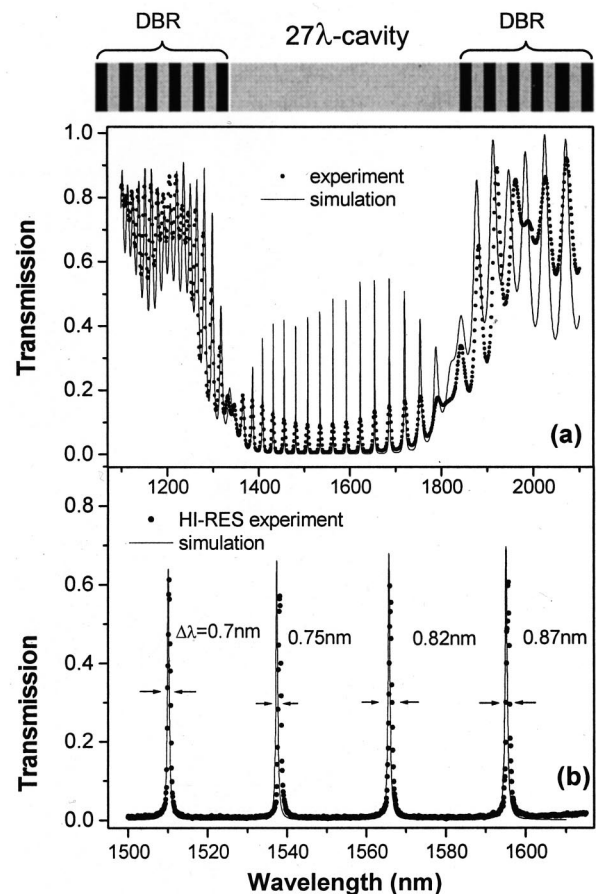


FIG. 9. Transmission spectra of a PS-based Fabry–Perot interference filter with  $27\lambda$  microcavity (dots) and the simulations (lines): (a) Wide range measurements with 1 mm spot size and (b) high-resolution measurement with  $35 \mu\text{m}$  diameter spot. The top diagram shows the structure of the thick microcavity.

thickness of the cavity layer, several optical modes can be sustained. We thus expect to observe several transmission peaks in the stop band region. Indeed, Fig. 9(a) shows a uniform distribution of transmission peaks. A more resolved measurement is shown in Fig. 9(b). Four narrow transmission peaks were observed in the wavelength range between 1.5 to  $1.6 \mu\text{m}$ . The Lorentzian fits to these transmission data give linewidth values of  $\Delta\lambda \sim 0.78 \text{ nm}$  ( $\pm 0.08 \text{ nm}$ ). These correspond to  $Q$  factors of more than 2000. We also show in both graphs, in Fig. 9, the numerical simulations for the structure (lines) which precisely fit the data. The fitting parameters were 1.5 and 2.13 for the  $n$  values for  $H$  and  $L$  layers, respectively, which are consistent with the values obtained from the analysis of the other structures. One can calculate the typical spacing  $\Delta\lambda_0$  between two modes at a certain  $\lambda_0$  by the following approximate formula:<sup>3</sup>

$$\Delta\lambda_0 \sim \frac{\lambda_0^2}{2nd}, \quad (1)$$

where  $n$  is the refractive index of the cavity and  $d$  the thickness. Eq. (1) gives  $\Delta\lambda_0 \sim 28.7 \text{ nm}$ , which is in good accordance with the experimental data.

We stress that the origin of the narrow multiple peaks in this thick cavity and in CMC structures are different: These

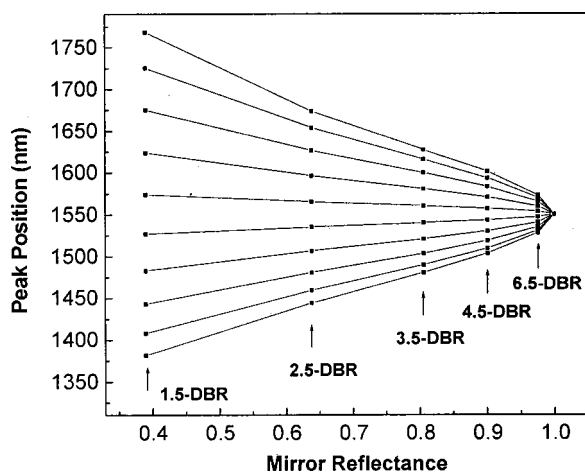


FIG. 10. Calculation of the transmission resonance modes for a ten coupled microcavity structure as a function of the reflectivity of the coupling internal mirror.

are multiple optical modes of a single cavity and splitting of the single cavity resonances due to the optical coupling of the various cavities, respectively. The signature of the physical difference is, in the former case, the uniform distribution of the peaks over the whole stop band, whereas in the latter case the peaks are densely packed around the resonance wavelength. The spacing of the transmission resonances for the CMC peaks depends on the optical coupling strength, which is provided by the reflectance of internal mirrors (number of DBR periods).<sup>12,13</sup> For two coupled cavities, the analytical expression shows an inverse dependence with the reflectance of the internal mirror.<sup>12</sup> For a larger number of coupled cavities, numerical calculations are necessary. Figure 10 reports the results of simulations for a ten CMC structure. The splitting increases as the coupling increases, i.e., as the reflectance of the internal mirror decreases. In the limit of no coupling between the cavities (100% reflecting mirrors), all ten modes are degenerate.

## VI. CONCLUSIONS

We have realized and optically characterized PS single and coupled cavity structures. A careful control of the etching parameters allows one to obtain high-quality free-standing multilayers. We demonstrate the possibility of obtaining very narrow transmission resonances with high transmission values for NIR wavelengths.  $Q$  factors as high as 3380 in a single  $\lambda$  microcavity and 2000 in thick-cavity structures are measured. It is very important to use small light spots to avoid the lateral doping inhomogeneities and to measure subnanometer wide resonances. The good agreement between the transmission data and simulations shows that the growth parameters are well controlled along the growth axes, which is responsible for the good optical characteristics of our very thick free-standing structures.

Angle-dependent measurements show a blueshift of the resonance peak for single microcavities. Splitting of TE and TM polarized modes is also observed due to birefringence of

the active layer. Therefore, PS microcavities can be utilized as band-pass filters with tunable peak position.

PS-based multilayer structures have potential applications in channel filtering within telecommunication devices with small insertion losses. The number and position of resonance peaks can be designed and their linewidths controlled in the NIR range of 1.5 to 1.6  $\mu\text{m}$ . In addition, the porous microstructure of the material allows infiltration of active media or liquid crystals, which opens many interesting applications of these structures for switching and electrically controlled band-pass filters. Moreover, the high sensitivity of PS to certain gases and vapors allows the use of these devices as optical sensors, where the narrowness of the peaks is essential to detect slight shifts of the spectrum.

## ACKNOWLEDGMENTS

The authors acknowledge A. Lui of ITC-IRST for the SEM micrographs. This work is supported by INFM with Project No. PAIS-RANDS 2001.

- <sup>1</sup>O. Bisi, S. Ossicini, and L. Pavesi, *Surf. Sci. Rep.* **38**, 1 (2000).
- <sup>2</sup>M. G. Berger, R. Arens-Fischer, M. Kruger, S. Billat, H. Luth, S. Hilbrich, W. Theiß, and P. Grosse, *Thin Solid Films* **297**, 137 (1997).
- <sup>3</sup>L. Pavesi, *Riv. Nuovo Cimento* **20**, 1 (1997).
- <sup>4</sup>S. Nagata, C. Domoto, T. Nishimura, and K. Iwameji, *Appl. Phys. Lett.* **72**, 2945 (1998).
- <sup>5</sup>S. Frohnhoff and M. G. Berger, *Adv. Mater. (Weinheim, Ger.)* **6**, 963 (1994).
- <sup>6</sup>V. Pellegrini, A. Tredicucci, C. Mazzoleni, and L. Pavesi, *Phys. Rev. B* **52**, 14328 (1995).
- <sup>7</sup>L. Pavesi, C. Mazzoleni, A. Tredicucci, and V. Pellegrini, *Appl. Phys. Lett.* **67**, 3280 (1995).
- <sup>8</sup>S. Chan and P. M. Fauchet, *Opt. Mater.* **17**, 31 (2001).
- <sup>9</sup>S. Chan and P. M. Fauchet, *Appl. Phys. Lett.* **75**, 274 (1999).
- <sup>10</sup>P. J. Reece, G. Lerondel, W. H. Zheng, and M. Gal, *Appl. Phys. Lett.* **81**, 4895 (2002).
- <sup>11</sup>J. Hecht, *Laser Focus World* **38**, 153 (2002).
- <sup>12</sup>L. Pavesi, G. Panzarini, and L. C. Andreani, *Phys. Rev. B* **58**, 15794 (1998).
- <sup>13</sup>M. Ghulinyan, C. J. Oton, Z. Gaburro, P. Bettotti, and L. Pavesi, *Appl. Phys. Lett.* **82**, 1550 (2003).
- <sup>14</sup>Z. Gaburro, N. Daldosso, L. Pavesi, G. Faglia, C. Baratto, and G. Sberveglieri, *Appl. Phys. Lett.* **78**, 3744 (2001).
- <sup>15</sup>S. Billat, M. Thönissen, R. Arens-Fischer, M. B. Berger, M. Krüger, and H. Luth, *Thin Solid Films* **297**, 22 (1997).
- <sup>16</sup>M. Born and E. Wolf, *Principles of Optics* (Cambridge University Press, Cambridge, UK, 1980).
- <sup>17</sup>C. J. Oton, L. Dal Negro, P. Bettotti, L. Pancheri, Z. Gaburro, and L. Pavesi, in *Radiation—Matter Interaction in Confined Systems*, edited by L. C. Andreani, G. Benedek, and E. Molinari (Società Italiana di Fisica, Bologna, 2002), p. 303.
- <sup>18</sup>C. Pichering, M. I. J. Beale, and D. J. Robins, *Thin Solid Films* **125**, 157 (1984).
- <sup>19</sup>F. Ferrieu, A. Halimaoui, and D. Bensahel, *Solid State Commun.* **84**, 293 (1992).
- <sup>20</sup>D. Kovalev, G. Polisski, J. Diener, H. Heckler, N. Künzner, V. Y. Timoshenko, and F. Koch, *Appl. Phys. Lett.* **78**, 916 (2001).
- <sup>21</sup>C. J. Oton, Z. Gaburro, M. Ghulinyan, L. Pancheri, P. Bettotti, L. Dal Negro, and L. Pavesi, *Appl. Phys. Lett.* **81**, 4919 (2002).
- <sup>22</sup>H. Münder, M. G. Berger, S. Frohnhoff, M. Thönissen, and H. Luth, *J. Lumin.* **57**, 5 (1993).
- <sup>23</sup>A. G. Cullis, L. T. Canham, and P. D. Calcott, *J. Appl. Phys.* **82**, 909 (1997).
- <sup>24</sup>V. M. Aroutiounian, M. Ghulinyan, and H. Tributsch, *Appl. Surf. Sci.* **162**, 122 (2000).